Anal. Bioanal. Electrochem., Vol. 16, No. 12, 2024, 1085-1097
https://www.doi.org/10.22034/abec.2024.719410

Analytical & Bioanalytical Electrochemistry

Full Paper

Octylamine Assisted Hydrothermal Growth of Silver Selenide Nanospheres as Efficient Electrode Material for Energy Storage Application

Sanghamitra Mohapatra, Tapan Kumar Sarangi, and Kusha Kumar Naik*

P.G. Department of Physics, Berhampur University, Odisha, Pin:760007, India

*Corresponding Author, Tel.: +91-7008789133
E-Mail: kkn.phy@buodisha.edu.in

Received: 30 October 2024 / Received in revised form: 3 December 2024 / Accepted: 16 December 2024 / Published online: 31 December 2024

Abstract- This study explores the electrochemical storage potential of Ag_2Se nanosphere electrode material synthesized via a hydrothermal method, demonstrating their applicability in supercapacitors. Comprehensive structural, morphological, and optical analyses were conducted using X-ray diffraction (XRD), scanning electron microscopy (SEM), and UV-visible spectroscopy, confirming the formation of Ag_2Se nanospheres. Supercapacitive performance was assessed through cyclic voltammetry (CV), galvanostatic charge-discharge (GCD), and electrochemical impedance spectroscopy (EIS) in a three-electrode configuration using KOH as the electrolyte. The Ag_2Se nanospheres exhibited high pseudocapacitive behavior, delivering a specific capacitance of 437.5 F/g, an energy density of 29.5 Wh/kg, and a power density of 89.32 W/kg, positioning them as effective energy storage materials. Notably, the nanospheres displayed remarkable cyclic stability, retaining 90% of their capacitance after 100 cycles, underscoring their durability for long-term applications. These findings suggest that Ag_2Se nanospheres offer a promising balance between high performance and cyclic stability, making them suitable candidates for advanced supercapacitor applications.

Keywords- Octylamine; Silver Selenide; Nanospheres; Supercapacitance; Hydrothermal

1. INTRODUCTION

The increasing energy demands have sparked intense research on renewable energy and energy storage systems that prioritize efficiency and performance without negatively impacting the ecosystem [1–3]. Energy storage systems such as batteries, fuel cells, and capacitors are

meeting power demands with suitable performance stability; however, there is still a significant energy demand to meet the prevailing challenges in energy application [4–6]. Electrochemical storage systems based on electrochemistry provide clean and renewable energy by transferring chemical energy to electrical energy through controllable chemical reactions [7,8]. Supercapacitors deal with electrochemical principles and provide high energy density and superior power density in a short span of time with rapid charge-discharge cycles compared to other energy storage devices like batteries, fuel cells, and capacitors [9–12]. The performance of a supercapacitor depends on the physicochemical features, like elemental composition, surface structure, structural geometry, electrical conductivity, and chemical nature of the materials [13,14]. Once again, the surface configuration of nanostructures and constituent elements significantly influences their energy storage performances. This has led to the design and optimization of the morphology and composition of nanomaterials, making them the ideal electrode materials for energy storage devices [15,16]. By engineering these parameters in suitable combinations, we can enhance the performance of a supercapacitor significantly.

Metal chalcogenides are getting more attention in research these days because they behave in different ways, are flexible, have a layer-like structure, are more conductive, work well as catalysts, have lower internal resistance, and have ohmic loss [17–19]. Also, selenide is often used as an active electrode material because it has a higher conductivity (1×10^{-3} Sm^{-1}) than sulfur (1×10^{-28} Sm^{-1}). This means that electrochemical reactions happen faster on the electrode's surface and carriers move faster as well [20]. Similarly, silver is the well-known transition metal for its conductivity and electrocatalytic nature. Because of these qualities, Ag_2Se is the best transition metal selenide for electrodes: it has strong oxidation states, redox pairs, high electroconductivity, thermochemical stability, and safety in the environment [21,22]. With Na_2SO_4 as the electrolyte, Shivasharma et al. looked at the orthorhombic structure of a thin film of silver selenide as an electrode material. A cyclic voltammetry test showed a specific capacitance of 112.4 F/g at a 10 mV/s scan rate, and a galvanostatic charge-discharge test showed a specific capacitance of 115.99 F/g at 0.8 A/g [23]. One more study by Shnag Wu et al. looked into the supercapacitive activity of NiSe/SnSe nanocomposite electrode material. They found that it had a specific capacitance of 116 mA h/g [24]. Based on the hydrothermal process, Gu et al. made the N-rGO/NiSe nanocomposite, which had a specific capacitance of 340.4 mA h/g at 1 A/g [25]. Similarly, Balasingam et al. reported a specific capacitance of 211 F/g of $MoSe_2$/rGO nanosheet synthesized by hydrothermal process [26], and Arul et al. synthesized $NiSe_2$ in a hydrothermal way and reported the specific capacitance of 75 F/g respectively [27]. Li et al. synthesized CuSe nanosheets in a solid-state method and reported the specific capacitance of 209 F/g [28]. Reviewing the above literature, pure and crystalline silver selenide could be synthesized in an economical process. The synthesis parameters not only determine the structural and morphological characteristics but also deliver material properties like supercapacitive charge storage. Therefore, we could use an easy

hydrothermal method to create silver selenide nanospheres, with octylamine facilitating the process. This would lead to enormous capacitance.

Usually, vapor-phase deposition methods such as physical vapor phase (PVD) and chemical vapor phase (CVD) synthesize chalcogenide materials to achieve high quality and purity. We reported a simple and inexpensive way to make Ag_2Se nanostructures with a monoclinic lattice. We used octylamine as the synthesis medium, a cost-effective hydrothermal method and scanning electron microscopy (SEM), X-ray diffraction (XRD), and UV-visible spectroscopy to check the Ag_2Se material's structure, shape, and optical properties. Then, an electrochemical setup with three electrodes shows the Ag_2Se nanostructure's electrochemical properties. The Ag_2Se nanostructure has a specific capacitance of 437.5 F/g at a scan rate of 1 mV/s from cyclic voltammetry (CV) and 433.5 F/g at a current density of 0.08 A/g, which shows that it can hold a charge or discharge for a long time.

2. EXPERIMENTAL SECTION

2.1. Material Synthesis

The simple and inexpensive hydrothermal method was used to make silver chalcogenide. Silver nitrate ($AgNO_3$), selenide powder (Se), and octylamine were used as the main ingredients. First, 0.2717 g (80 mM) of $AgNO_3$ was mixed with 10 ml of octylamine. In a separate beaker, 0.0256 g (40 mM) of selenide powder was also mixed with 10 ml of octylamine. Both of these mixtures were stirred for 20 minutes. Next, we mixed both solutions and moved them to a 25 ml autoclave, where they underwent a 16 hour heat treatment at 423 K. At high temperatures, the dissolved ‘Ag and Se’ ions reduced and oxidized through interaction by gaining thermal energy and reacted with themselves, leading to the nucleation and phase transformation of Ag_2Se molecules. Then, each nucleated Ag_2Se molecule stuck together by intramolecular force, which was controlled by the synthesis parameters. This made Ag_2Se nanoparticles. eared precipitated solution at room temperature for the characterization and supercapacitor study of the synthesized material. Figure 1 depicts the synthesis procedure of the synthesized Ag_2Se material to enhance understanding and visualization of the process.

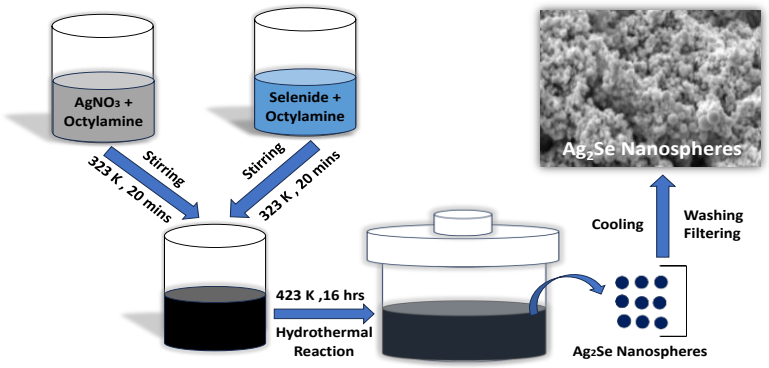

Figure 1. Schematic representation of synthesis process of the Ag_2Se nanospheres

2.2. Material Characterization

An X-ray diffractometer (PROTO AXRD using Cu-K_α radiation, $\lambda = 1.54$ Å) was executed to determine the crystal structure and crystallite size of the as-synthesized material, and the morphology was examined using a SEM (Flex-SEM 1000). The optical band gap of the produced material was determined by a UV-visible spectrophotometer (Labtronics, Model LT-2201).

2.3. Electrochemical measurement

The electrochemical measurements for the supercapacitor study were conducted using a potentiostat (Sinsil International Ltd.) in a three-electrode configuration setup taking 1 M of KOH as an electrolyte. We used a glassy carbon electrode with silver selenide that had been synthesized and pasted with Nafion as the working electrode. A platinum wire was used to collect the current, and Ag/AgCl was used as the reference electrode. The CV experiment was performed at a potential window ranging from a potential of -0.6 V to 0.2 V with diverse scan rates to identify the redox potential of the Ag_2Se material. Similarly, GCD tests were completed at various current densities in the -0.6 V to 0.2 V voltage range with the time parameter. The electrochemical impedance spectroscopy (EIS) measurement was performed in the frequency range from 100 kHz to 0.01 Hz to observe the electrochemical characteristics of the electrode material. Using cyclic voltammetry and galvanostatic charge-discharge plots, the specific capacitance of silver chalcogenide material was calculated using equations (1) and (2), as follows:

$$Cs = \frac{1}{2 \times m \times v \times \Delta V} \int_{Va}^{Vb} i(v) dV \quad (1)$$

$$Cs = \frac{i \times \Delta t}{m \times \Delta V} \quad (2)$$

where ‘i’ is the current in (A),'m’ is the mass of the electrode material in (0.1 mg), ‘Δt’ is the discharge time in (s), scan rate is in (mV/s), and potential window is in (V).

3. RESULTS AND DISCUSSION

3.1. Structural investigation

The structural analysis of Ag_2Se was obtained using an X-ray diffractometer, and its diffracted XRD pattern is supplied in Figure 2(a), which revealed that the characteristic peaks of Ag_2Se material are sharpened, distinct, and distinguishable at angles (2θ) having Miller indices (-102), (012), (110), (-113), (-121), (-122), (120), (-104), (031), (-202), (-121), (-124), (-214), (014), (-215), (-142), (-233), (-106), and (-135), respectively. The high-pitched characteristic peaks of the Ag_2Se indicate crystallinity, and all the observed peaks obtained at different angles are assigned to the Ag_2Se material (JCPDS card 01-075-1061). No other peaks

except Ag_2Se material are recognized, which demonstrated that the grown material is pure and highly crystalline in nature.

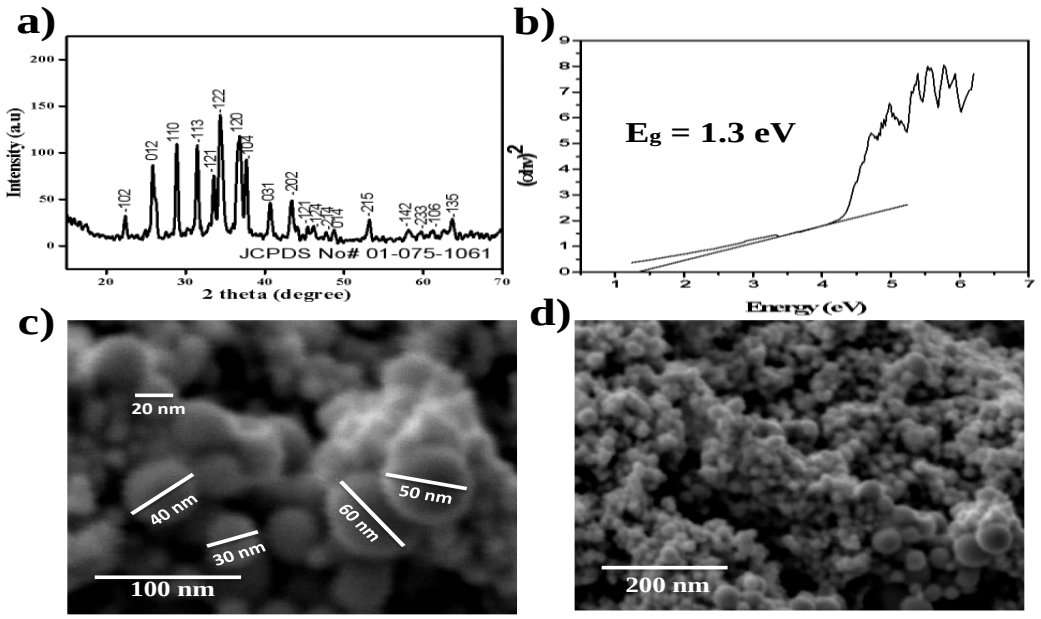

Figure 2. (a) XRD pattern of Ag_2Se material; (b) Band gap of Ag_2Se material; (c) SEM image of Ag_2Se nanospheres; (d) SEM image of Ag_2Se nanospheres

Similarly, the band gap of the synthesized Ag_2Se material was calculated using a UV-Vis spectrometer and found to be 1.3 eV, which is semiconducting in nature, as shown in Figure 2(b). Due to the semiconducting nature of the synthesized material, it would facilitate more charge storage kinetics and exhibit improved supercapacitive performance. The morphological feature of the Ag_2Se material was obtained by executing SEM analysis, as shown in Figure 2(c-d), identifying the morphology of the synthesized material as having a nanosphere like structure. The nanospheres are constructed uniformly in nature, and the dimensions of the nanospheres are determined to be 20–60 nm. The nanospheres are distinct and clearly distinguishable from each other. The nanospheres are homogeneous and uniformly grown with significantly controllable growth kinetics and synthesis parameters. It is obvious that the nanospheres exhibit more electrochemical energy storage kinetics due to their large specific surface area, electron confinement, short electron transport path, and easy surface functionalization mechanics, which is a good gesture for supercapacitor application. Also, to evaluate the uniformity and distribution of elements in the synthesized silver selenide (Ag_2Se) electrode material, elemental mapping was carried out using Energy-Dispersive X-ray Spectroscopy (EDS) integrated with Scanning Electron Microscopy (SEM). The elemental maps for silver (Ag) and selenium (Se) demonstrate a homogeneous distribution of both elements throughout the electrode matrix, confirming the successful synthesis of Ag_2Se, as shown in Figure S1. The uniformity in the distribution of Ag and Se is critical for ensuring

consistent electrochemical performance. This homogeneity minimizes charge transport resistance and maximizes the active sites available for redox reactions, leading to improved charge storage capacity. Furthermore, the absence of elemental segregation or clustering indicates the structural stability of the synthesized material, which is essential for achieving long term cycling stability in supercapacitor applications.

3.2. Electrochemical performance

The electrochemical storage performance of the Ag_2Se nanospheres is determined by performing a CV and GCD experiment taking three electrode configurations set up and 1 M of KOH electrolytic solution. At first the potential window of the material was finalized by performing the CV at a scan rate of 20 mV/s, then CVs of different rates were executed successively. The broad oxidation peak and reduction peak were obtained, suggesting the redox behavior of the Ag_2Se nanospheres, Figure 3(a). The current intensity of the redox peak decreased with the decreasing scan rates, maintaining the potential window the same, indicating the homogeneous electrocatalytic behavior of the synthesized Ag_2Se nanosphere material. Due to the redox performance of the nanosphere, it is concluded that the nanosphere would possess pseudocapacitive behavior.

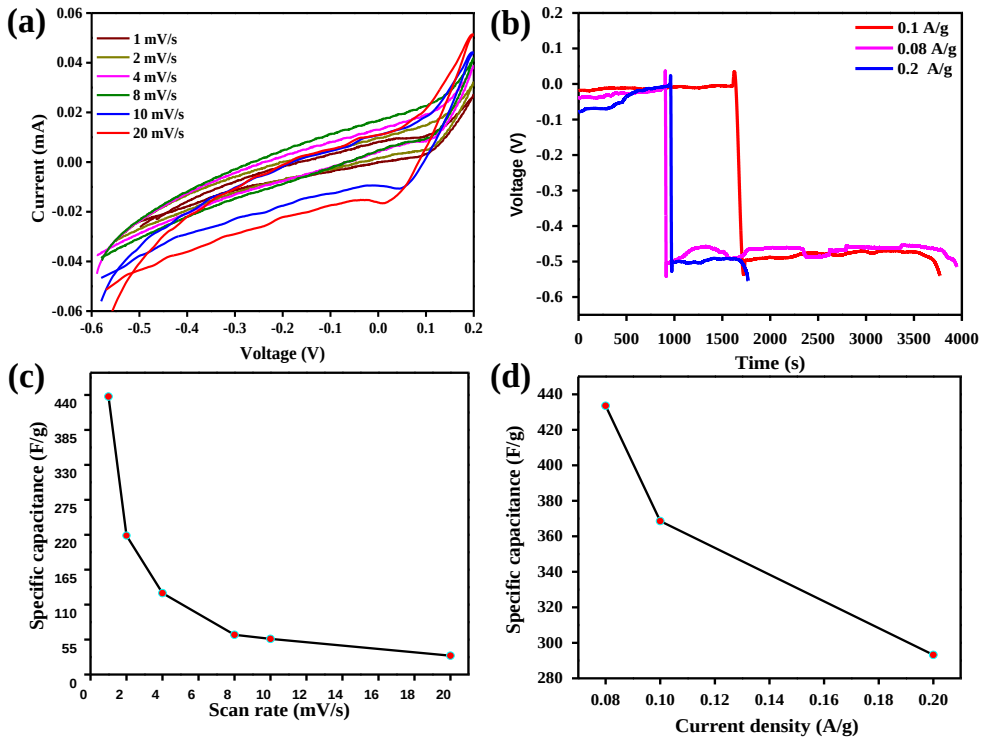

Figure 3. (a) CV curves of Ag_2Se nanospheres at different scan rates; (b) GCD curves of Ag_2Se nanospheres at different current densities; (c) specific capacitance performance of the synthesized nanospheres with various scan rates; (d) Plot between specific capacitances with various current densities

From the CV graph plotted at Figure 3(a), it clearly demonstrates that the intensity of current increases with the increase in scan rates, and the area enclosed by CV curves also increases simultaneously; as a result, the specific capacitance of the Ag_2Se nanospheres decreases eventually, as shown in Figure 3(c). The decrease in specific capacitance of the nanosphere with the increase in scan rates may be explained by enhanced ion diffusion and electrode surface accessibility, which are caused by the high surface area of the nanomaterial [29]. At lower scan rates, ions present in the electrolyte solution have more time to diffuse into the surface of the nanosphere. As a result, a large amount of charge is stored at the electrode-electrolyte interface, leading to higher capacitance. Similarly, at a lower scan rate, a large number of electrolyte ions interact and access the active nanosphere present on the electrode surface; as a result, the specific capacitance of the Ag_2Se nanospheres increases effectively. More participation of active ions with the active molecules of the nanospheres indicates more storage capacity and supercapacitive performance [30]. Another reason may be the reduction in double-layer charging and minimization of the polar effect. At slower scan rates, the charging process is more likely to be dominated by the formation of a true electrical double layer at the electrode-electrolyte interface rather than charging through faradaic processes. The capacitance associated with the double layer is typically higher than that associated with faradaic reactions [31]. Similarly, slower scan rates can help minimize polarization effects such as concentration polarization or ohmic drop, which can limit the effective capacitance of an electrode at higher scan rates [32]. Table 1 displays the calculated specific capacitance of Ag_2Se nanospheres using equation (1) from the CV curve.

Table 1. The specific capacitance of Ag_2Se nanospheres at different scan rates

Scan rate (mV/s)	1	2	4	8	10	20
Specific capacitance (F/g)	437.5	218.7	128.1	62.5	56.2	29.6

Figure S2 specifies the CV graph of Ag_2Se electrode measured in various concentrations but at constant scan rate of 20 mV/s. The result revealed that the specific capacitance is highest in 0.5 M KOH compared to 1.0 M KOH. However, when the concentration is increased to 1.5 M KOH, the specific capacitance decreases, as shown in Table S1. This trend can be attributed to the influence of electrolyte concentration on ion availability and ionic conductivity. At lower concentrations, such as 0.5 M KOH, the electrolyte provides an optimal number of hydroxide ions (OH^-), ensuring efficient interaction with the electrode surface and facilitating charge storage. However, at higher concentrations (1.5 M KOH), the excessive ionic strength leads to increased viscosity and reduced ionic mobility. This hinders the diffusion of OH^- ions into the porous structure of the electrode, thereby limiting the effective utilization of the active material and reducing specific capacitance.Additionally, the high concentration of KOH may cause

partial blockage of the electrode's active sites due to excessive ion crowding, further contributing to the decline in capacitance.

Figure 3 (b) demonstrates the GCD curve of Ag_2Se nanospheres performed at various current densities, which revealed the charging and discharging performance of the Ag_2Se nanospheres. The charging time of the nanosphere is determined to be 15 s, and the discharging time is 30 s, respectively, which is good for supercapacitor application. Figure 3(d) specifies the relation between current charge density and specific capacitance of the nanospheres, which demonstrates that the specific capacitance of the nanosphere decreases with the increase in current density. There are a number of factors that affect specific capacitance. The first is electrochemical effects [33]. In this effect, higher current densities can induce electrochemical reactions within the nanosphere, such as oxidation or reduction of active species at the electrode-electrolyte interface. These reactions can alter the effective surface area available for charge storage and can lead to degradation of the electrode material, reducing its overall capacitance. The second effect is ion migration [34]. Actually, increased current density can cause accelerated ion migration within the material. This phenomenon may lead to ion trapping or polarization effects, which interfere with the efficient storage and release of charge, ultimately reducing the specific capacitance. The third effect that reduces specific capacitance is concentration polarization [30]. Here, at higher current densities, the concentration of ions near the electrode surface can become depleted due to rapid ion transport. This concentration polarization can hinder the charge storage process, diminishing the effective capacitance of the material. Lastly, electrical resistance plays a vital role in that higher current densities often result in increased electrical resistance within the material due to factors such as ion transport limitations or joule heating effects. Elevated resistance can impede the efficient charging and discharging of the capacitor, reducing its overall capacitance [35]. The specific capacitance of Ag_2Se nanospheres is calculated using equation 2 from Figure 3(b), and the results are given in Table 2.

Table 2. The specific capacitances of Ag_2Se nanospheres at different current densities

Current densities (A/g)	0.08	0.1	0.2
Specific capacitance (F/g)	433.5	368.5	293.2

Figure 4(a) shows the graph between energy density and power density of Ag_2Se nanospheres, which gives a decent value of energy and power density so that the material can be suitable for supercapacitor applications. High power density gives information about the rapid charging and discharging of supercapacitors. This is particularly important where quick energy transfer and backup power systems are required, such as burst power delivery in

electronic devices. The synthesized Ag_2Se nanospheres hold the most advantages regarding supercapacitor applications due to their high power density with moderate energy density, i.e., a longer life cycle than batteries, and we can also design this supercapacitor in a compact form. Figure 4(b) shows the first five cycles of charging and discharging times of the Ag_2Se nanospheres. Similarly, Figure 4(c) shows the charging and discharging times of the nanosphere for the last five cycles, and approximately the same charging and discharging of the nanosphere is recorded.

To check the stability in electrochemical performance of the synthesized Ag_2Se nanospheres, a GCD experiment of 100 cycles has been performed, and the same charging and discharging nature of the graph of the Ag_2Se nanosphere electrode material is recorded. So, 90% of the retention of supercapacitance performance, even after 100 cycles, is recorded in Figure 4(d), which is admirable.

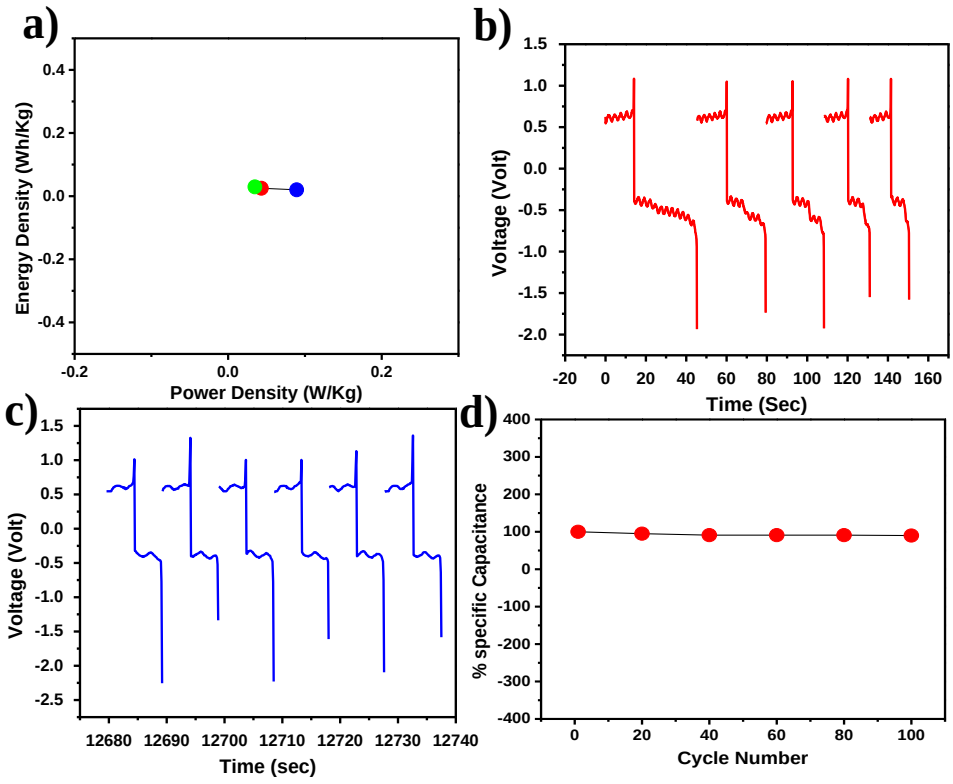

Figure 4. (a) Plot between Power Density with Energy density; (b) Charge and discharge time of Ag_2Se of first five cycles; (c) Charge and discharge time of Ag_2Se of last five cycles; (d) Plot between specific capacitances with various cycle numbers

The EIS of the Ag_2Se nanosphere is carried out over a frequency range from 100 kHz to 0.01 Hz at open circuit potential to detect the frequency response of the Ag_2Se nanosphere. Figure 5(a), a Bode plot of Ag_2Se electrode material, shows the phase angle is -64.4 degrees, which confirms the capacitive nature of the electrode material, and the Figure 5(b) Nyquist plot shows the frequency response of Ag_2Se electrode material. The impedance spectra possess a

vertical line at low frequency, which signifies the nanosphere electrode material is capacitive in nature with a fast rate of ion diffusion.

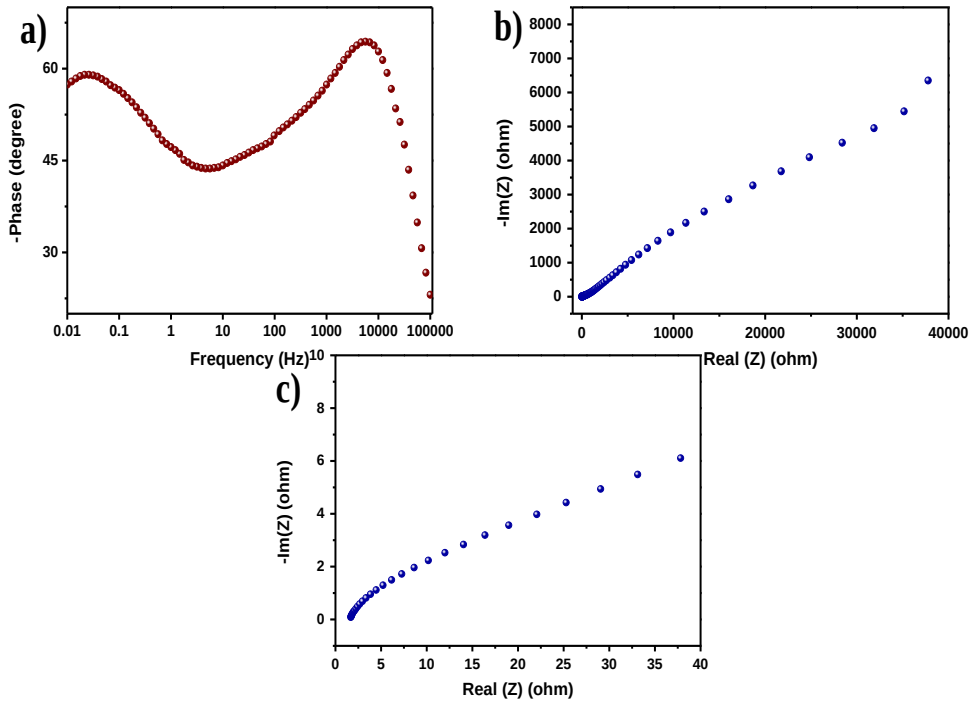

Figure 5. (a) Bode plot of Ag_2Se at frequency range 0.01Hz to 100kHz; (b) Nyquist plot of Ag_2Se; (c) Magnified view of Nyquist plot of Ag_2Se electrode material

Table 3. Comparison table of specific capacitances of Ag_2Se nanospheres with other selenide materials

Composition	Techniques	Specific capacitance (F/g)	Reference
NiSe–Se	CVD	271.9	[36]
NiSe /$SnSe_2$	Hydrothermal	116	[24]
N-rGO/$NiSe_2$	Hydrothermal	340.4	[25]
Ag_2Se	SILAR	115.9	[23]
$MoSe_2$/rGO	Hydrothermal	211	[26]
$NiSe_2$	Hydrothermal	75	[27]
CuSe	Solid state	209	[28]
Ag_2Se	Hydrothermal	437.5	Present work

Based on the magnified view of this plot, Figure 5(c), in the high-frequency region, a very small semicircle is also explored, which indicates there is a restriction in charge transfer at the electrode-electrolyte interface with negligible resistance of solution.

The energy storage capacitance of the synthesized Ag_2Se nanospheres is compared with the similar transition selenide materials available in the literature, as shown in Table 3, and excellent specific capacitance is recorded.

4. CONCLUSION

In this study, we have synthesized silver selenide (Ag_2Se) nanospheres using a cost-effective hydrothermal method, employing octylamine as the growth medium. The material was thoroughly characterized via XRD, SEM, and UV-visible spectroscopy, confirming its crystalline structure and nanosphere morphology. Its electrochemical properties were evaluated in a three-electrode setup with KOH as the electrolyte.

- *Key Findings:*
    - Achieved a specific capacitance of 437.5 F/g at a scan rate of 1 mV/s.
    - Energy density of 29.5 Wh/kg and power density of 89.32 W/kg.
    - Retained 90% capacitance after 100 cycles, demonstrating excellent cyclic stability.
- *Limitations:*
  The specific capacitance decreases with higher scan rates and current densities, likely due to ion transport and polarization effects. The long-term stability over thousands of cycles remains unexplored.
- *Suggestions for Future Work:*
  Future research should focus on optimizing synthesis parameters to enhance performance at higher current densities, exploring other electrolytes to improve ionic mobility, and extending cycling tests to evaluate long-term durability in real-world applications.

Acknowledgments

This research was made possible through the support of the OURIIP project (OURIIP-21SF/PH/67), funded by OSHEC, Government of Odisha, and the SERB project (EEQ/2022/000147), sponsored by the Department of Science and Technology, Government of India. The experimental studies were conducted at the P.G. Department of Physics and the Center of Excellence (CoE) at Berhampur University.

Declarations of interest

The authors declare no conflict of interest in this reported work.

REFERENCES

[1] N. De Nevers, Air pollution control engineering, Waveland Press (2010).
[2] M. Jaccard, Sustainable fossil fuels: the unusual suspect in the quest for clean and enduring energy, Cambridge University Press (2006).
[3] D.J. Soeder, Fossil fuels and climate change, Fracking and the Environment: A Scientific Assessment of the Environmental Risks from Hydraulic Fracturing and Fossil Fuels, 1st Edition, Springer (2021) pp. 155–185.
[4] S.A. Mousavi, M. Mehrpooya, and M.R. Ganjali, Mater. Chem. Phys. 320 (2024) 129394.
[5] S.A. Mousavi, M. Mehrpooya, and M.R. Ganjali, Int. J. Hydrogen Energy 51 (2024) 787.
[6] H. Kamali, M. Mehrpooya, S.A. Mousavi, and M.R. Ganjali, New J. Chem. 46 (2022) 18351.
[7] S. Glasstone, An introduction to electrochemistry, Read Books Ltd. (2011).
[8] C.G. Zoski, Handbook of Electrochemistry, Elsevier (2007).
[9] S.S. Karade, A. Agarwal, B. Pandit, R.V. Motghare, S.A. Pande, and B.R. Sankapal, J. Colloid Interface Sci. 535 (2019) 169.
[10] S.S. Karade, B.R. Sankapal, J. Electroanal. Chem. 802 (2017) 131.
[11] C.D. Jadhav, S.S. Karade, B.R. Sankapal, G.P. Patil, and P.G. Chavan, Chem. Phys. Lett. 723 (2019) 146.
[12] J. Theerthagiri, K. Karuppasamy, G. Durai, A. Rana, P. Arunachalam, K. Sangeetha, P. Kuppusami, and H. Kim, Nanomaterials 8 (2018) 256.
[13] R. Boddula, A. Khan, A.M. Asiri, and A.E. Kolosov, Handbook of Supercapacitor Materials. Wiley Online Library (2022).
[14] K.K. Kar, Handbook of nanocomposite supercapacitor materials II. vol. 302. Springer; (2020).
[15] M.A. Scibioh, and B. Viswanathan, Materials for supercapacitor applications, Elsevier (2020).
[16] S. Ratha, and A.K. Samantara, Supercapacitor: instrumentation, measurement and performance evaluation techniques, Springer (2018).
[17] Kk. Devarayan, J. Park, H.Y. Kim, and B.S. Kim, Carbohydr Polym 163 (2017) 153.
[18] B. Pandit, V.S. Devika, and B.R. Sankapal, J. Alloys Compd. 726 (2017) 1295.
[19] A.I. Oje, A.A. Ogwu, M. Mirzaeian, A.M. Oje, and N. Tsendzughul, Appl. Surf. Sci. 488 (2019) 142.
[20] A. Abouimrane, D. Dambournet, K.W. Chapman, P.J. Chupas, W. Weng, and K. Amine, J. American Chem. Soc. 134 (2012) 4505.
[21] C. Ji, Y. Zhang, T. Zhang, W. Liu, X. Zhang, H. Shen, Y. Wang, W. Gao, Y. Wang, J. Zhao, and W.W. Yu, The Journal of Physical Chem. C 119 (2015) 13841.

[22] H. Mołnås, S.J. Paul, M.R. Scimeca, N. Mattu, J. Zuo, N. Parashar, L. Li, E. Riedo, and A. Sahu, Cryst Growth Des. 24 (2024) 2821.
[23] T.K. Shivasharma, L.K. Bommineedi, B.R. Sankapal, Inorg. Chem. Commun. 135 (2022) 109083.
[24] S. Wu, S. Zhou, Q. Feng, H. Zhao, X. Xu, T. Cui, H. Zhang, X. Wang and Q. Yang, J. Energy Storage 42 (2021) 103032.
[25] Y. Gu, L.Q. Fan, J.L. Huang, C.L. Geng, J.M. Lin, M.L. Huang, Y.F. Huang, and J. Wu, J. Power Sources 425 (2019) 60.
[26] S.K. Balasingam, J.S. Lee, and Y. Jun, Dalton Transactions 45 (2016) 9646.
[27] N.S. Arul, and J.I. Han, Mater. Lett. 181 (2016) 345.
[28] L. Li L, J. Gong, C. Liu, Y. Tian, M. Han, Q. Wang, W. Zhu, X. Hong, Q. Ding, and J. Bao, ACS Omega 2 (2017) 1089.
[29] K.W. Nam, and K.B. Kim, J. Electrochem. Soc. 149 (2002) A346.
[30] A. Eftekhari, J. Mater. Chem. A Mater. 6 (2018) 2866.
[31] E. Faggioli, P. Rena, V. Danel, X. Andrieu, R. Mallant, and H. Kahlen, J. Power Sources 8 (1999) 261.
[32] P. Bhojane, J. Energy Storage 45 (2022) 103654.
[33] C. Zhong, Y. Deng, W. Hu, D. Sun, X. Han, J. Qiao, and J. Zhang, Electrolytes for electrochemical supercapacitors. CRC Press (2016).
[34] J.W. Graydon, M. Panjehshahi, D.W. Kirk, J. Power Sources 245 (2014) 822.
[35] J. Chen, P.S. Lee, Adv. Energy Mater. 11 (2021) 2003311.
[36] S. Subhadarshini, E. Pavitra, R. Rama, N.R. Chodankar, D.K. Goswami, Y.K. Han, and N.C. Das, ACS Appl Mater Interfaces 12 (2020) 29302.